

# Analysis of Magnetic Force Linearity in Magnetic Levitation Systems

**Samed Gumus and Yavuz Ozturk**

Department of Electrical and Electronics Engineering, Ege University  
35100 Izmir, Turkey  
91220001780@ogrenci.ege.edu.tr, yavuz.ozturk@ege.edu.tr

---

*Abstract: The important parameters of bar magnet configurations, in which the same poles are facing each other, are investigated with a focus on their potential applications in magnetic levitation. The scalar product of the magnetic field and its gradient between magnets is referred to as  $fz$ , which is a function for force calculations. The magnitude and linear range of this function are then examined. These parameters are computed for several air gap lengths between the magnets, as well as the height and thickness of the magnets, while keeping the magnet length constant. The calculations are experimentally validated by measuring the magnetic field of a magnet system. The choice of thickness and height of the magnet was found to have critical effects on both linearity and the maximum value of  $fz$  within the linear range. The results of this study can be used to guide the selection of magnet dimensions and also to evaluate the factors that can influence the measurements and sensitivity of magnetic levitation systems.*

*Keywords: bar rectangular magnet; magnetic force linearity; magnetic levitation*

---

## 1 Introduction

Specific types of permanent magnet systems have been subject to many researches and key components of many applications such as magnetic levitation [1-4], separation [5], flow focusing [5] [6], tilt or displacement sensor technologies [7], motor designs [8], control [9], detection applications in polymers [10], and biomedical technologies [11] [12]. In addition, magnetic fields generated by them, and the interactions between the magnets [13-15] have become the subject of numerous research studies, from education [16] to new areas of applications [17] [18].

Magnets with different well-known geometries can be used in many systems such as rectangular prism [11] [13], Halbach array [19], cylinder [20] [21], sphere [9], ring [18], and cone [22]. These kinds of magnets, when integrated with a magnetic field sensor, can be used to measure displacement or position, making them

particularly advantageous in applications where precise position information is critical—such as in control systems [23] and robotics [24]. The magnetic field created by these magnets can be analytically calculated [25-28]. In particular, combinations of the bar magnets (rectangular prism shaped) have been found in many fascinating applications such as magnetic levitation [11], separation, flow focusing [5], density measurements [11] [19], and crack detection [29]. For this reason, the studies about investigation of magnet systems by using analytical calculations, simulations and/or experiments gives valuable contributions to mentioned [30] and future new applications [4] [17].

The magnetic levitation systems of two magnet systems in repulsion, same poles facing each other, have been found in magnetic levitation applications as one of the active research areas. In these systems, magnets in the form of a cylindrical or rectangular prism provide levitation of paramagnetic particles in diamagnetic medium or diamagnetic particles in a paramagnetic medium [4]. The form of the magnetic field in magnetic levitation systems for the density measurements is important for sensitivity and density measurement range [1] [2]. Many studies in this area generally have been focused on application and not magnetic characteristics [9, 12, 13, 20] and theoretical studies on these systems are found to be limited. In many of these studies, the magnetic field or magnetic forces in interest were assumed to be linear [11, 12, 20] although linearity of these functions highly depends on magnet dimensions and their spacing [1]. These magnetic system parameters also have a high influence on magnetic force. As a consequence, especially at the initial steps of designing magnetic systems for the mentioned applications, investigating, calculating or having insights on the effects of magnet parameters on the magnetic force and its linearity are found to be crucial.

A key motivation for this study is to demonstrate that linear magnetic fields—and the resulting forces—are strongly influenced by magnet positioning and physical parameters. In many applications, including magnetic levitation [3] [4], sensor design [31], and actuator systems [32] [33], magnets are often used under the assumption of linear magnetic field behavior, frequently without a supporting theoretical foundation. However, this assumption holds true only under specific conditions, which necessitates a thorough examination and clarification of these limitations. The findings of this study are expected to enhance both the efficiency of future applications in these areas and the interpretation of previous research. Moreover, the combined analysis of magnetic field linearity and maximum force magnitude may provide valuable insights for systems that employ symmetric magnets as sensors or sources of magnetic force. To the best of our knowledge, this work is the first to investigate linear range approximations in relation to magnet system parameters.

In this study, the product of magnetic field and magnetic field gradient in the axis at the center of two bar magnets, same poles facing each other, is investigated theoretically and experimentally. The results of linearity analysis and maxima of this function in terms of magnet system dimensions are presented. The aim of this

study is to give insight on the influence of magnet parameters on the value and form of magnetic forces and help to select correct magnets for applications needed in many areas such as biomedical and material technologies.

The remainder of the paper is organized as follows. Section 2 provides a theoretical explanation of the linear magnetic field in a symmetrical magnet system and outlines the methodological approach used for the analysis. Section 3 presents the analysis results and an example application based on various magnet parameters, and discusses them in the context of related studies. Finally, Section 4 summarizes the conclusions and highlights the study's contributions.

## 2 Theory and Method

### 2.1 Theory

In magnetic levitation systems, which are the focus of this study, it is important to operate under linear force conditions to obtain precise measurements and ensure accurate interpretation [1]. Although the concepts of linearity and nonlinearity have numerous definitions and applications across scientific disciplines [34], in the context of this study, linearity is defined as a relationship between input and output in which a change in input results in a proportional change in output. An ideal linear system produces an output that remains consistently proportional to the input across its operating range, typically represented by a first-order (linear) polynomial function. This characteristic is crucial for accurate system modeling, precise calibration, and reliable performance in control and measurement applications [35].

In magnetic levitation systems, the force equation for diamagnetic particles in a paramagnetic fluid or vice versa can be expressed by the following equation [11] [36].

$$V \frac{\Delta\chi}{\mu_0} \mathbf{B}\nabla\mathbf{B} = V g_e \Delta\rho \quad (1)$$

The following notations are used in (1);  $\Delta\chi$  is the magnetic susceptibility difference of the medium ( $\chi_m$ ) and the particle ( $\chi_c$ ) to be levitated,  $\mathbf{B}$  is the magnetic field (magnetic flux density, magnetic induction),  $\mu_0$  is the magnetic permeability of free space,  $V$  is the particle volume,  $g_e$  is the gravitational acceleration of Earth, and  $\Delta\rho$  is the density difference of the medium and the particle. When this system is used for density measurement, the factor that determines position of the levitated particles for constant parameter values of the medium will be the  $\mathbf{B}\nabla\mathbf{B}$  function. In equation (1), the term  $\mathbf{B}\nabla\mathbf{B}$  can be adjusted by magnet parameters. This term denotes an expression that is ideally expected to be linear in the direction of the levitated axis [4, 11, 37]. In the following section, this term is examined for the system given in Figure 1, which consists of magnets in the form of rectangular

prisms and the same poles are facing each other. In Figure 1a, the geometry of magnets and magnetic field the gaussmeter used for magnetic field measurements (Lakeshore DSP 455 gaussmeter) was shown. Levitation takes place along the  $z$ -axis for similar systems and therefore it was chosen to express the magnetic force ( $F_B$ ), using (1), in this axis (Figure 1b) with the following equations.

$$F_B = V \frac{\Delta\chi}{\mu_0} f_z \quad \text{and} \quad f_z = B_z \frac{\partial B_z}{\partial z} \quad (2)$$

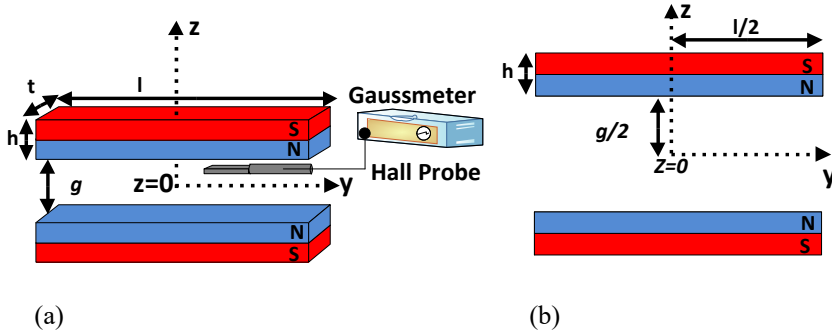


Figure 1

The schematics of the magnet system and measurement setup(a), and schematics of coordinate axis with respect to the magnets (b)

Both the experimental measurements were taken, and numerical calculations were made on the axis at the midpoints of the rectangular prism magnets shown in Figure 1b. The magnetic field  $B$  of a single rectangular magnet on the  $z$ -axis is given in (3) [25, 26] for the single magnet given in Figure 2. In equation (3),  $t$ ,  $l$ ,  $h$  symbols refer to thickness, length and height of the magnet, respectively.

$$B(z) = \frac{\mu_0 M}{\pi} \left[ \arctan \left( \frac{(t/2)(l/2)}{(z-h/2)\sqrt{(t/2)^2+(l/2)^2+(z-h/2)^2}} \right) - \arctan \left( \frac{(t/2)(l/2)}{(z+h/2)\sqrt{(t/2)^2+(l/2)^2+(z+h/2)^2}} \right) \right] \quad (3)$$

Here,  $M$  is the magnetization magnitude of the magnet. In Figure 2, different from the two magnet systems in Figure 1, the origin of the coordinate system is in the magnet center.

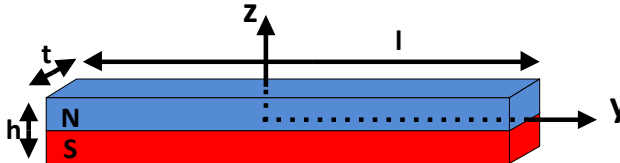


Figure 2

Dimensions and reference system of a rectangular prism magnet

As shown in Figure 1b, the  $z=0$  point is chosen as the midpoint of the two magnets; therefore, it is convenient to express the magnetic field of each magnet by shifting the function of the single magnet  $B$  given in (3) by  $\Delta$  where  $\Delta$  is  $(h/2 + g/2)$ . Consequently, the magnetic field functions of the first and second magnet become  $B_{1z}(z) = B(z - \Delta)$  and  $B_{2z}(z) = -B(z + \Delta)$ , respectively. Taylor series expansion of the first magnet is:

$$B_{1z}(z) = B(z - \Delta) = \sum_{k=0}^{\infty} \frac{B_{1z}^{(k)}(0)}{k!} (z)^k = a_0 - a_1z + a_2z^2 - a_3z^3 + \dots \quad (4)$$

Taylor series expansion of  $B$  for the second magnet is:

$$B_{2z}(z) = -B(z + \Delta) = \sum_{k=0}^{\infty} \frac{B_{2z}^{(k)}(0)}{k!} (z)^k = -a_0 - a_1z - a_2z^2 - a_3z^3 + \dots \quad (5)$$

Where in equations (4) and (5),  $B_{1z}(0) = B(\Delta)$ ,  $B_{2z}(0) = -B(\Delta)$ , and  $B^{(k)}$  is the  $k$ th derivative of  $B$ . Since  $B$  is even function  $B(\Delta) = B(-\Delta)$  the even degrees of  $z$  simplify and only odd degrees of  $z$  components remain in the sum of  $B_{1z}(z)$  and  $B_{2z}(z)$  polynomials as in (6):

$$B_z = B_{1z}(z) + B_{2z}(z) \cong -2a_1z - 2a_3z^3 \quad (6)$$

The terms after the third degree can be neglected for small  $z$  values in the polynomial of  $B_z$ . If the approximation of  $B_z$  in (6) is used, the term  $f_z$  can be found as follows:

$$f_z \approx (-2a_1z - 2a_3z^3) \frac{d(-2a_1z - 2a_3z^3)}{dz} = 4a_1^2z + 16a_1a_3z^3 + 12a_3^2z^5 \quad (7)$$

The expression in (7) is required to be linear for many applications and it is close to linear for small  $z$  values depending on the coefficients  $a_1$  and  $a_3$ . As the  $z$  values increase, the coefficients of the third and higher power (order) terms become dominant. For linear  $f_z$  and linear force, it is important to set magnet parameters and distance between magnets so that  $a_1 a_3$  product and  $a_3^2$  terms are small.

## 2.2 Linearity Analysis of $f_z$

Analysis was carried out to determine in which regions the  $f_z$  function, which determines the magnetic force as in (1), is approximately linear as shown in (8). Using (3), the sum of each magnet's magnetic field ( $B_z$ ) and  $f_z$  were calculated in the axis of the air gap region of the two magnet systems shown in Figure 1b. In magnetic levitation studies, the magnet length should be significantly greater than its height and thickness to ensure that the forces acting on the particles along the magnet are symmetrical, and that the force variation remains low in the region near the center axis of the magnet ( $x = 0, y = 0$ ). Therefore, a magnet length of  $l=50$  mm was chosen, which is close to the standard length of capillary tubes or microchannels where the samples are placed [38]. The calculations were made for the gap  $g$  values of 1.5 mm, 3 mm and 5 mm, the height  $h$  and thickness  $t$  values, were taken in the range of 0.5-10 mm with 0.1 mm steps. For all calculations, a

magnetization value of  $M = 1000$  kA/m was used, as it is close to that of high-grade N35 magnets (930–970 kA/m) and low-grade N45 magnets (1050–1100 kA/m). "fit" function of a linear polynomial was used in MATLAB to find parameters of the linear model for  $f_z$ . One of the parameters, the root mean squared error (*rmse*) was utilized for testing whether the calculated data fits a linear model [39]. The *rmse* formula is given in the equation below.

$$rmse = \sqrt{\frac{\sum_{i=1}^n (\hat{y}_i - y_i)^2}{n}} \quad (8)$$

In equation (8),  $\hat{y}_i$  is the *i*th fitted linear function value,  $y_i$  is the *i*th calculated value of the function  $f_z$  at that point, and *n* is the total number of function values. The *n*=1000 value was set out for each calculation. The small value of *rmse* indicates that the fitted data converge to the linear function. To find maximum linear range first the fit range was started from the air gap value, and if the *rmse* value was greater than  $1 \text{ T}^2/\text{m}$ , the fit range was narrowed. Linear range was determined from the fit range when the first  $rmse \leq 1 \text{ T}^2/\text{m}$  condition was met. Figure 3 presents a flowchart that summarizes the steps of the analysis.

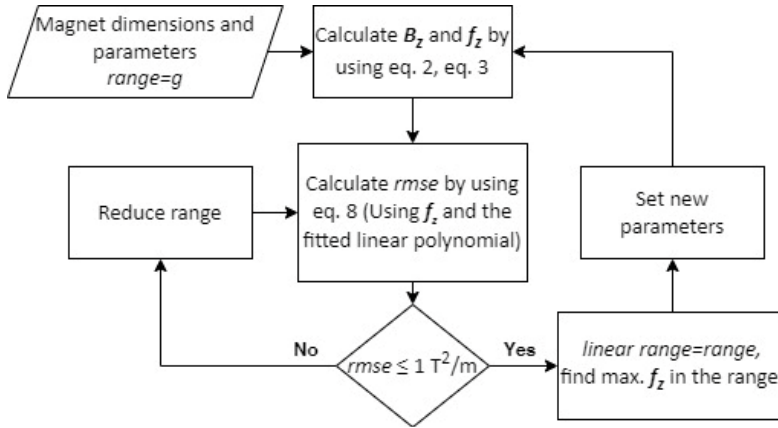


Figure 3

Flow chart of the linearity analysis

The calculated  $f_z$  values, along with the corresponding linear fit functions and linear ranges obtained from the algorithm (Figure 3) for two different sets of magnet dimensions, are shown in Figure 4. When magnet sizes and air gap *g* value are not selected appropriately, linear range becomes relatively small compared to air gap (Figure 4a). However, as shown in Figure 4b, when more suitable values are selected, both the  $f_z$  magnitude in the linear range and the linear range values increase. It is seen that the residual values (difference between calculated data and fitted function) are less than  $10 \text{ T}^2/\text{m}$  for  $g=1$  mm and  $169 \text{ T}^2/\text{m}$  for  $g=5$  mm. But, for both magnets, the linear range residual values are less than  $3 \text{ T}^2/\text{m}$ . Of course, it is possible to choose larger *rmse* values to expand the linear range depending on the

application. This study was carried out to show the effect of the magnet dimensions and air gap on the  $f_z$ . For this reason, results were obtained with the chosen  $rmse$  value of  $1 \text{ T}^2/\text{m}$  and analysis was made from the corresponding data.

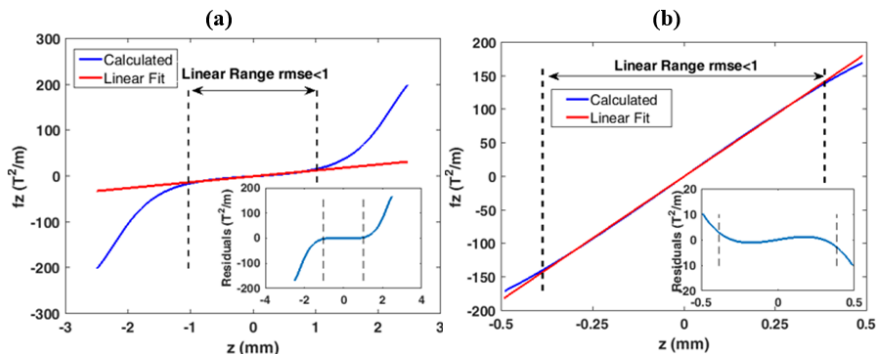


Figure 4

Plot of calculated and linear fitted  $f_z$  functions ( $rmse < 1$ ) with respect to  $z$  axis, for magnet dimension of  $l=50 \text{ mm}$ ,  $t=2 \text{ mm}$ ,  $h=5 \text{ mm}$ ; (a)  $g=5 \text{ mm}$ , (b)  $g=1 \text{ mm}$  (Insets: plots of residuals)

### 3 Results and Discussion

For many levitation studies such as density measurement of polymers or cells, linear magnetic force is desired to ease calculations and increase accuracy [1, 10, 11]. However, the magnetic forces are approximately linear in the certain ranges for the magnet systems as shown in equations (8) and (1). Therefore, for these kinds of systems, a detailed examination of the magnetic force might be crucial to increase sensitivity and for correct measurements [1, 3, 6, 8, 36]. For this purpose, analyses were made with this motivation to examine the selected parameters for the rectangular magnet configuration. In the analyses, the linear range of the  $f_z$  and the maximum  $f_z$  values within this linear range were investigated.

Contour and 3D plots of the linear range with respect to thickness ( $t$ ) and height ( $h$ ) for air gap length ( $g$ ) of  $1.5 \text{ mm}$ ,  $3 \text{ mm}$  and  $5 \text{ mm}$  are given in Figure 5. In these calculations the length of the magnet was kept constant as  $50 \text{ mm}$  and  $h$ ,  $t$  values of the magnets were changed with  $0.1 \text{ mm}$  intervals. The detailed investigation on the influence of magnet dimension on the  $B$  field of a single bar magnet can be found in the study of [26]. In their study, uniformity of  $B$  field magnitude in the center and boundaries of the magnet were shown to increase with the increase of  $l/h$  ratio [26]. So, the choice of  $l=50 \text{ mm}$  long magnet also satisfies the uniformity of  $B$  field along  $y$  direction. The maximum linear range was determined to satisfy  $rmse < 1 \text{ T}^2/\text{m}$ . It is worth mentioning that this  $rmse$  value can be chosen smaller or larger according to the application's requirements. Although this linear range determination approach

is for a particular condition, it shows the influence of  $h$ ,  $t$  and  $g$  parameters on investigated quantities.

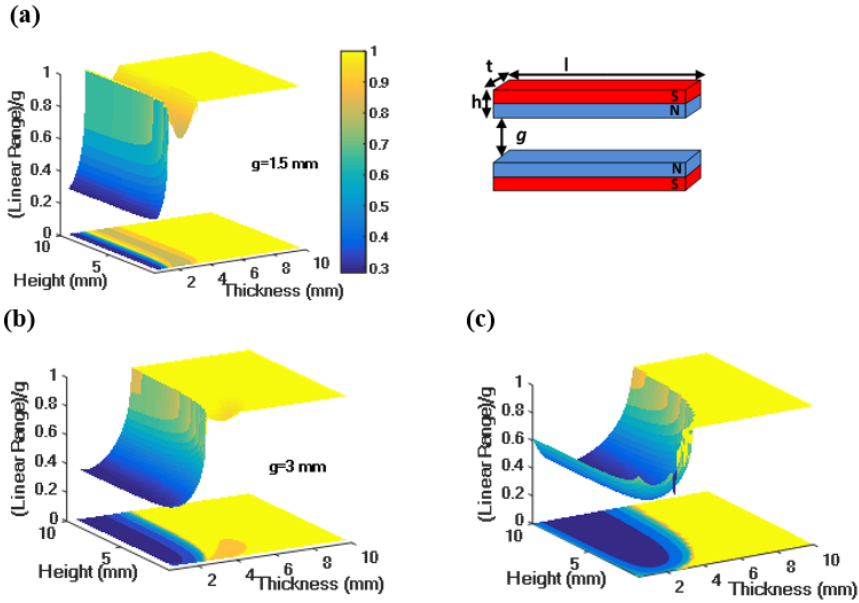


Figure 5

Plots of Linear Range ( $rmse < 1$ ) with respect to height and thickness of magnets a: for 1.5 mm air gap b: for 3 mm air gap; c: for 5 mm air gap. (Inset: magnet dimensions)

The results clearly reveal that the dimensions of both the magnet and the air gap play an important role in determining the range in which the  $f_z$  can be considered linear. Outside this region, the third or higher order terms of  $z$  become dominant for the  $f_z$  function as shown in Figure 4 and (7). The height  $h$  value, especially when it is longer than  $g$ , appears to be less effective compared to  $t$  and  $g$ . Thickness of magnets plays an important role when it is smaller than  $g$  but after its value much higher than  $g$  it becomes not effective and linear range becomes equal to  $g$ . According to the results the  $t$  thickness of the magnet could be chosen closer ( $g=3$  mm and  $g=5$  mm) or higher than  $g$  ( $g=1.5$  g) when linear range is considered. For  $g=1.5$  mm when  $t > g$  there is local minimum of the linear range around minimum value of  $0.84g$  which is acceptable for most of the levitation applications. By considering this, when  $t$  values selected to be higher than  $g$  (around  $1.4g$ ) acceptable linear range can be achieved. The air gap length  $g$ , could be narrowed within the limits of the application, to have a larger linear range in air gap, especially for small thickness  $t$  values.

The highest magnetic force value that can be produced in the linear range is also an important factor. It is especially crucial in measurement of high-density materials and also low paramagnetic ion requirements in biomedical applications [11] [40].

When the magnetic force term in (1) is higher the difference of densities in buoyant force can be larger. As a result, higher densities can be measured. As another example, in biomedical applications, it is recommended to use liquids with  $Gd^{3+}$  paramagnetic ion concentrations up to 100 mM [11] [40]. Especially since the  $\chi_m$  value is directly proportional to the paramagnetic ion content, the low  $\chi_m$  value decreases the  $\Delta\chi$  value in (1) and so relatively high  $f_z$  values is required for such applications.

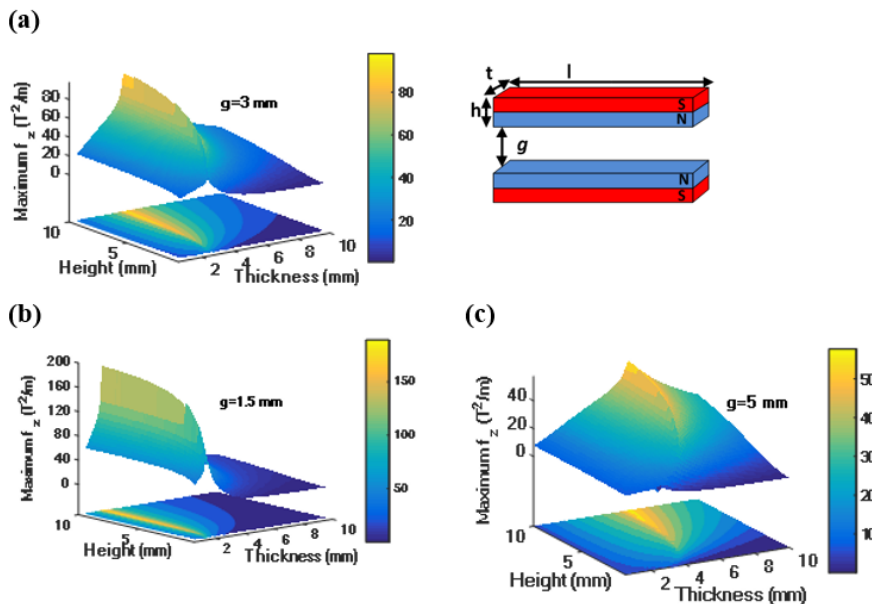


Figure 6

Maximum  $f_z$  in the linear range with respect to  $h$  and  $t$  a: for 3mm air gap, b: for 1.5 mm air gap; c: for 5 mm air gap ( $rmse < 1$ )

Contour and 3D plots of maximum  $f_z$  in the linear range for sets of  $t$  and  $h$  were presented in Figure 6 for several  $g$  values. As seen in Figure 6, the thickness is a critical parameter and for each height value there is a maximum of  $f_z$  at a certain thickness value. The trace of these maximum (yellow region in contour plots) well matches with the linear range contour plots where the maximum linear range obtained for lowest values of  $h$  and  $t$ . Not as critical as thickness but the height of magnets ( $h$ ) also has an important influence. It can be seen, that the maximum value increases as the  $h$  value increases, except points near to the local maximums (tip of shark's fin like plots). Other design parameters or constraints for applications should be taken into account when choosing the height of magnets. For example, in optical systems using mirrors and lenses, the choice of long magnets will limit the use of lenses due to their limited focal length and magnification needs as in studies of Anil-Inevi et al [40]. Local maximum of with respect to height  $h$  also observed for various values of thickness. These maximums observed at the tip of shark's fin

like plots can be used for applications when the need for magnet dimensions is small. For example, the local maximum value of  $f_z = 161 \text{ T}^2/\text{m}$  for  $g = 1.5 \text{ mm}$  and at  $h = 2.9 \text{ mm}$ ,  $t = 2 \text{ mm}$  can be used for such designs. Another conclusion from the plots is the maximum  $f_z$  in the linear gap decreases, while the air gap widens for the same magnet dimensions. If Figure 5 and Figure 6 are examined together, the tip of shark fin (Figure 6) and the boundary of where linear range equals to  $g$  first time, for lower values of  $t$  (Figure 5), intersects. So, choosing  $t$  and  $h$  values, on the tip of the shark fin of Figure 6, will both satisfy linear range and maximum  $f_z$  conditions.

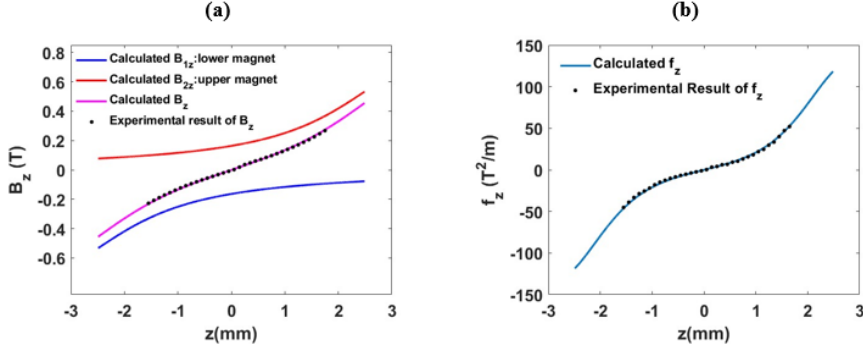


Figure 7

a:  $B_z$  measurements and theoretical results and calculated b:  $f_z$  results for 5 mm air gap and  $62 \times 12 \times 3$  mm magnet dimensions

To experimentally validate equations (2) and (3), the calculated and measured values of the magnetic field ( $B_z$ ) were compared on a selected magnet set. The magnet set, consisting of two magnets with dimensions of  $62 \times 12 \times 3 \text{ mm}$  ( $l \times h \times t$ ), was placed as shown in Figure 1. Measurements were taken using a Hall effect sensor, and due to the limitation of the Hall sensor dimensions, measurements were conducted for a relatively large magnet separation of 5 mm. The Hall sensor was placed along the  $z$ -axis of the coordinate plane shown in Figure 1b, and the axis was scanned in 0.05 mm steps. The calculated  $B_{1z}$  and  $B_{2z}$  values of each magnet and their sum ( $B_z$ ), along with the measurement results, are all shown in Figure 7a. A magnetization of  $M = 920 \text{ kA/m}$ , which corresponds to the magnetization value for a typical M35 magnet, was found by fitting the measured and calculated data. As can be seen from the figure, both the measured and calculated data match well. It can also be observed that the measurement results are in accordance with the polynomial function specified in equation (7). After a certain value of  $z$ , the third or higher-order terms in (7) become dominant, making the nonlinearity of the  $f_z$  function more distinct (Figure 7b).

According to the given results, the length of the air gap should be selected less than 3 mm in order to obtain a linear range equal to the entire air gap. To show this,  $B_z$  and  $f_z$  values are calculated with respect to  $z$  for 5, 3 and 1.5 mm gap values and given in Figure 8. As seen in the figure, narrowing the gap between magnets, the maximum  $B_z$  and  $f_z$  values decreases, while the linearity of the  $f_z$  increases.

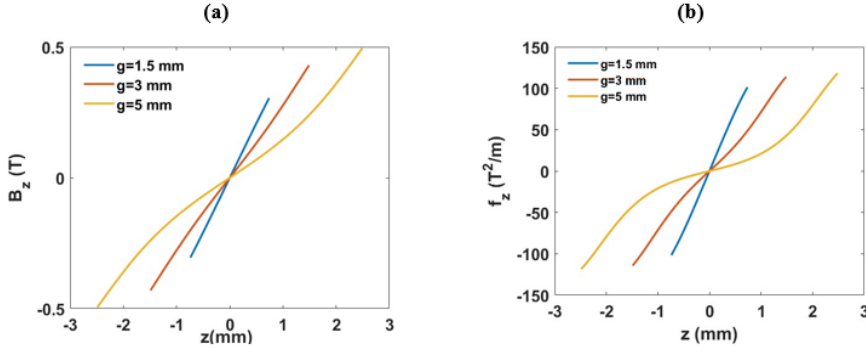


Figure 8

Theoretical results of a:  $B_z$  and b:  $f_z$  for 1.5, 3, 5 mm air gap length and the magnet dimensions of 62x12x3 mm

The following section demonstrates an example application of magnetic levitation in density measurement, highlighting the strong dependence of linear approximation accuracy on system parameters. Using (1), the density of particles or cells  $\rho_c$  in a paramagnetic fluid with known density  $\rho_m$  can be calculated from measurements of position with respect to the  $z = 0$  reference point. Assuming that the  $f_z$  varies linearly with  $z$ , the expression:  $f_z \approx 4a_1^2 z = bz$  (Equation 7) can be used, and Equation (1) simplifies to [1]:

$$\rho_c = \rho_m - \frac{\chi_m f_z}{\mu_0 g_e} \approx \rho_m - b \frac{\chi_m}{\mu_0 g_e} z \quad (9)$$

For 100 mM  $Gd^{3+}$  solution, the following values were used for calculations:  $\rho_m = 1020 \text{ kg/m}^3$ ,  $\chi_m = 3.2 \cdot 10^{-5}$ ,  $g_e = 9.81 \text{ m/s}^2$ ,  $\mu_0 = 4\pi \cdot 10^{-7} \text{ Tm/A}$ . For a magnet pair of size 62x12x6 mm with magnetization of  $M = 920 \text{ kA/m}$ , the linear range of  $f_z$  (Figure 4) and its linear coefficient  $b$  were obtained using the algorithm presented in the flowchart (Figure 3). The approximate particle/cell density  $\rho_c$  was first calculated using this linear approximation using (9). Subsequently, a more accurate calculation of  $\rho_c$  was performed using equations (2) and (3) and (9) without linear approximation. The difference between the two results defines the density error, and the maximum errors were computed both within the linear range and across the entire range (g).

As shown in Table 1, the value of  $b$  increases with decreasing  $g$ , indicating stronger magnetic forces in the linear region. In applications targeting a wider density range, a stronger magnetic force is preferred [1], since the measurable density range is limited by the boundaries at  $z = \pm g/2$  in Equation (9). Within this range, the particle with minimum density reaches equilibrium at  $z = +g/2$ , while the particle with maximum density reaches equilibrium at  $z = -g/2$ . It is worth noting that there is a trade-off between measurable range and sensitivity, in which the value of  $b$  should be carefully considered.

The linear range was defined using a threshold of  $rmse < 1$ , resulting in  $rmse$  values equal to 1 for all cases except  $g = 2$  mm. The linear range was also found to be a nonlinear function of  $g$ . It equaled  $g$  at  $g = 2$  mm, and was smaller than  $g$  at all other values in Table 1. Maximum density error was observed outside the linear range (Figure 4), and this error increased with decreasing  $g$ , except at the optimal value  $g = 2$  mm. These results demonstrate that the proposed algorithm can effectively determine both the maximum linear range and the minimum density error (residual). This analysis is particularly valuable in applications requiring high measurement accuracy—such as the density-based differentiation of cancerous and healthy cells—where the acceptable error margin is typically below  $10 \text{ kg/m}^3$  [41]. The presented example further illustrates that, with appropriate selection of magnetic parameters and gap distance, linear approximations can be reliably used to measure density with negligible error.

Table 1  
Linear approximation parameters of  $f_z$  and maximum density errors

<b>g (mm)</b>	<b>b (<math>f_z \simeq bz</math>) (<math>10^3 \text{ T}^2/\text{m}^2</math>)</b>	<b><i>rmse</i> (<math>\text{T}^2/\text{m}</math>)</b>	<b>Linear range (mm)</b>	<b>Maximum density error in linear range (<math>\text{kg}/\text{m}^3</math>)</b>	<b>Maximum density error in g (<math>\text{kg}/\text{m}^3</math>)</b>
<b>5</b>	19.2	1	2.1	7.2	184.8
<b>3</b>	63.9	1	1.5	6.7	53.6
<b>2</b>	112.1	0.57	2	6.5	6.5
<b>1.5</b>	143.8	1	1.4	7.5	13.3

## Conclusions

In this study, a system of two rectangular prism magnets, placed face to face and aligned at the same poles (essential in many magnetic levitation systems), was examined. The product of the magnetic field and its gradient,  $f_z$ , and its linearity, which is an important function to calculate magnetic force, was investigated at the axis centered between magnets. Theoretical and experimental results are presented to show the influence of the system parameters of magnet height, magnet thickness, and air gap length on the magnetic field and  $f_z$  in the target region. As a result, it was found that it would be appropriate to choose both height and thickness values higher than the gap length  $g$  to obtain reasonable  $f_z$  and optimum linear range of  $f_z$ . And for constant air gap value, height  $h$  can be selected much higher than  $g$  to increase maximum  $f_z$  in linear range. It was also concluded that it is possible to increase  $f_z$  value in the linear region by decreasing air gap or increasing height of the magnets and choosing optimal thickness value. We believe that the study will be especially useful for the magnet selection for several sensor and density measurement applications, where the linearity of magnetic forces is considered.

## Acknowledgements

The authors of this study would like to thank Dr. Oğuz Gürses for helpful discussions and editing the manuscript. This work has been supported by The Scientific and Technological Research Council of Turkey (TUBITAK) under Grand 121S903.

## References

- [1] Zhang, C., Zhao, P., Wen, W., Xie, J., Xia, N., Fu, J.: Density measurement via magnetic levitation: Linear relationship investigation, *Polymer Testing*, 2018, 70, pp. 520-525
- [2] Xie, J., Zhao, P., Jing, Z., Zhang, C., Xia, N., Fu, J.: Research on the sensitivity of magnetic levitation (MagLev) devices, *Journal of Magnetism and Magnetic Materials*, 2018, 468, pp. 100-104
- [3] Nemiroski, A., Kumar, A. A., Soh, S., Harburg, D. V., Yu, H.-D., Whitesides, G. M.: High-sensitivity measurement of density by magnetic levitation, *Analytical Chemistry*, 2016, 88(5), pp. 2666-2674
- [4] Lyu, C., Tang, D., Zhang, C., Xie, J., Zhang, Q., Nie, J., He, Y., Fu, J., Wang, J., Zhao, P.: Magnetic levitation for non-contact manipulation and measurement of cells, *Sensors and Actuators B: Chemical*, 2023, 385, p. 133692
- [5] Xuan, X.: Recent advances in continuous-flow particle manipulations using magnetic fluids, *Micromachines*, 2019, 10(11), p. 744
- [6] Luo, L., He, Y.: Magnetically induced flow focusing of non-magnetic microparticles in ferrofluids under inclined magnetic fields, *Micromachines*, 2019, 10(1), p. 56
- [7] Öztürk, Y., Yarici, I.: Research on a novel magnetic tilt sensor designed using Hall elements and ferrofluid, *Journal of Electrical Engineering*, 2019, 70(5), pp. 406-411
- [8] Szabó, G., Veszprémi, K.: FEM parameterized sensorless vector control of permanent magnet synchronous machines using high-frequency synchronous voltage injection method, *Acta Polytechnica Hungarica*, 2022, 19(9), pp. 117-140
- [9] Bojan-Drăgoc, C.-A., Radac, M.-B., Precup, R.-E., Hedrea, E.-L., Tănăsioiu, O.-M.: Gain-scheduling control solutions for magnetic levitation systems, *Acta Polytechnica Hungarica*, 2018, 15(5), pp. 89-108
- [10] Xie, J., Zhao, P., Zhang, C., Fu, J., Turng, L.-S.: Current state of magnetic levitation and its applications in polymers: A review, *Sensors and Actuators B: Chemical*, 2021, 333, p. 129533
- [11] Delikoyun, K., Yaman, S., Yılmaz, E., Sarıgil, O., Anil-Inevi, M., Telli, K., Yalcin-Ozuysal, O., Ozcivici, E., Tekin, H. C.: HologLev: A hybrid

- magnetic levitation platform integrated with lensless holographic microscopy for density-based cell analysis, *ACS Sensors*, 2021, 6(6), pp. 2191-2201
- [12] Andersen, M. S., Howard, E., Lu, S., Richard, M., Gregory, M., Ogembo, G., Mazor, O., Gorelik, P., Shapiro, N. I., Sharda, A. V., Ghiran, I.: Detection of membrane-bound and soluble antigens by magnetic levitation, *Lab on a Chip*, 2017, 17(20), pp. 3462-3473
- [13] Gassner, A.-L., Abonnenc, M., Chen, H.-X., Morandini, J., Josserand, J., Rossier, J. S., Busnel, J.-M., Girault, H. H.: Magnetic forces produced by rectangular permanent magnets in static microsystems, *Lab on a Chip*, 2009, 9(16), p. 2321
- [14] Rovers, J. M. M., Jansen, J. W., Lomonova, E. A.: Analytical calculation of the force between a rectangular coil and a cuboidal permanent magnet, *IEEE Transactions on Magnetics*, 2010, 46(6), pp. 1656-1659
- [15] González, M. I.: Forces between permanent magnets: experiments and model, *European Journal of Physics*, 2016, 38(2), p. 025202
- [16] Asato, K., Teruya, K., Nagado, T., Tamaki, S.: Development of magnetic levitation system for science and technology education: magnetic levitation control by using a Hall element displacement sensor with neural network, *Electrical Engineering in Japan*, 2017, 200(2), pp. 51-60
- [17] Sozmen, A. B., Arslan-Yildiz, A.: Utilizing magnetic levitation to detect lung cancer-associated exosomes, *ACS Sensors*, 2024, 9(4), pp. 2043-2049
- [18] Xia, L., Liu, J., Zhu, X., Liu, R., Wen, H., Cao, Q.: Asymmetric magnetic levitation for density-based measurement and analysis, *Analytica Chimica Acta*, 2024, 1287, p. 341951
- [19] Gao, Q.-H., Yan, G., Zou, H.-X., Zhang, W.-M., Peng, Z.-K., Meng, G.: Density-based measurement and manipulation via magnetic levitation enhanced by the dual-Halbach array, *IEEE Sensors Journal*, 2020, 20(4), pp. 1730-1737
- [20] Ashkarran, A. A., Gharibi, H., Zeki, D. A., Radu, I., Khalighinejad, F., Keyhanian, K., Abrahamsson, C. K., Ionete, C., Saei, A. A., Mahmoudi, M.: Multi-omics analysis of magnetically levitated plasma biomolecules, *Biosensors and Bioelectronics*, 2023, 220, p. 114862
- [21] Panina, L. V., Gurevich, A., Beklemisheva, A., Omelyanchik, A., Levada, K., Rodionova, V.: Spatial manipulation of particles and cells at micro- and nanoscale via magnetic forces, *Cells*, 2022, 11(6), p. 950
- [22] Hart, S., Hart, K., Selvaggi, J. P.: Analytical expressions for the magnetic field from axially magnetized and conically shaped permanent magnets, *IEEE Transactions on Magnetics*, 2020, 56(7), pp. 1-9

- [23] Szakács, T.: Pneumatic piston control modelling and optimization, *Acta Polytechnica Hungarica*, 2023, 20(6)
- [24] Pozna, C., Precup, R. E.: Aspects concerning the observation process modelling in the framework of cognition processes, *Acta Polytechnica Hungarica*, 2012, 9(1), pp. 203-223
- [25] Camacho, J. M., Sosa, V.: Alternative method to calculate the magnetic field of permanent magnets with azimuthal symmetry, *Revista Mexicana de Física E*, 2013, 59(3), pp. 8-17
- [26] Xiao-fan, G., Yong, Y., Xiao-jing, Z.: Analytic expression of magnetic field distribution of rectangular permanent magnets, *Applied Mathematics and Mechanics*, 2004, 25(3), pp. 297-306
- [27] Ravaud, R., Lemarquand, G., Lemarquand, V., Depollier, C.: Analytical calculation of the magnetic field created by permanent-magnet rings, *IEEE Transactions on Magnetics*, 2008, 44(8), pp. 1982-1989
- [28] Petruska, A. J., Abbott, J. J.: Optimal permanent-magnet geometries for dipole field approximation, *IEEE Transactions on Magnetics*, 2012, 49(2), pp. 811-819
- [29] Edwards, C., Palmer, S. B.: The magnetic leakage field of surface-breaking cracks, *Journal of Physics D: Applied Physics*, 1986, 19(4), p. 657
- [30] Szedlak-Stinean, A. I., Precup, R. E., Petriu, E. M., Roman, R. C., Hedrea, E. L., Bojan-Dragos, C. A.: Extended Kalman filter and Takagi-Sugeno fuzzy observer for a strip winding system, *Expert Systems with Applications*, 2022, 208, p. 118215
- [31] Park, W., Chun, H., Nguyen, P., Lee, C.: A differentially amplified Hall effect displacement sensor for positioning control of a long-range flexure stage, *Review of Scientific Instruments*, 2023, 94(7)
- [32] Sciuto, G. L., Bijak, J., Kowalik, Z., et al.: Displacement and magnetic induction measurements of energy harvester system based on magnetic spring integrated in the electromagnetic vibration generator, *Journal of Vibration Engineering & Technologies*, 2024, 12, pp. 3305-3320 <https://doi.org/10.1007/s42417-023-01045-w>
- [33] Bae, S. J., Lee, S. J., Joo, M. G., Im, D. J.: Dual magnet solenoid actuator: Practical applications, *Sensors and Actuators A: Physical*, 2024, 365, p. 114893
- [34] Venczel, M., Veress, Á., Peredy, Z.: Development of a viscosity model and an application for the filling process calculation in visco-dampers, *Acta Polytechnica Hungarica*, 2023, 20(7)
- [35] Pozna, C., Precup, R. E., Földesi, P.: A novel pose estimation algorithm for robotic navigation, *Robotics and Autonomous Systems*, 2015, 63, pp. 10-21

- [36] Dunne, P., Hilton, J., Coey, J.: Levitation in paramagnetic liquids, *Journal of Magnetism and Magnetic Materials*, 2007, 316(2), pp. 273-276
- [37] Zhang, C., Zhao, P., Gu, F., Zhang, X., Xie, J., He, Y., Zhou, H., Fu, J., Turng, L.-S.: Axial-circular magnetic levitation: A three-dimensional density measurement and manipulation approach, *Analytical Chemistry*, 2020, 92(10), pp. 6925-6931
- [38] Ince, O. D., Tekin, H. C.: MagSity platform: A hybrid magnetic levitation-based lensless holographic microscope platform for liquid density and viscosity measurements, *Lab on a Chip*, 2025
- [39] Yan, L., Zhao, T., Xie, X., Precup, R. E.: OSSEFS: An online semi-supervised ensemble fuzzy system for data streams learning with missing values, *Expert Systems with Applications*, 2024, 255, p. 124695
- [40] Anil-Inevi, M., Yaman, S., Yildiz, A. A., Mese, G., Yalcin-Ozuysal, O., Tekin, H. C., Ozcivici, E.: Biofabrication of in situ self-assembled 3D cell cultures in a weightlessness environment generated using magnetic levitation, *Scientific Reports*, 2018, 8(1), p. 7239
- [41] Gumus, S., Sabour-Takanlou, M., Bölükbaşı, G., Sabour-Takanlou, L., Ozturk, Y., Vardarlı, A. T., Guneri, P., Gurses, B. O., Karaca, B., Boyacioğlu, H.: Theoretical analysis of magnetic levitation technique and in vivo validation on oral cancer diagnosis, *Proceedings of the 2024 IEEE 14<sup>th</sup> International Conference on Nanomaterials: Applications & Properties (NAP)*, 2024, pp. 1-5